The Electrochemical Behavior of α,β′-Brass in Basic $NaNO_3$ Solutions

C. Berne,[a,b,c,*] E. Andrieu,[b] J. Reby,[c] J-M. Sobrino,[d] and C. Blanc[b,,z]**

[a] *Joint Laboratory CETIMAT, CETIM – CIRIMAT, 31030 Toulouse Cedex 4, France*
[b] *Université de Toulouse, CIRIMAT, UPS/INPT/CNRS, Equipe MEMO ENSIACET, BP 44362, 31030 Toulouse Cedex 4, France*
[c] *CETIM, Pôle Matériaux Métalliques et Surface, 44326 Nantes Cedex 3, France*
[d] *CETIM, Pôle Matériaux Métalliques et Surface, 60304 Senlis Cedex, France*

The electrochemical behavior of an α,β′-brass CuZn40Pb2 (CW617N) was studied in basic nitrate solutions with various basic pHs and nitrate ion concentrations. In all the chosen experimental conditions, corrosion at the open circuit potential proceeded by the galvanic coupling of the α and β′ phases, leading to a surface dezincification of the β′ phase. The study showed that the extent of the dezincification was affected by the presence of lead in the alloy but the pH was the major parameter. During polarization tests, a pseudo-passive or a passive stage followed by a breakdown was observed: corrosion phenomena mainly involved copper and zinc dissolution from the β′ phase. At pH 11, a Cu_2O/PbO layer was efficient in achieving passivity of the brass. At pH 12, a $Cu(OH)_2$-rich surface layer was formed: it was not protective enough, and complete dissolution of the β′ phase was observed leading to the removal of lead particles.
[DOI: 10.1149/2.0181512jes]

In various corrosive environments, α,β′-brasses, used in components in gas distribution networks, are believed to be susceptible to simultaneous dissolution (Cu, Zn) and/or selective dissolution (Zn, dezincification) processes. These phenomena are expected to play a major role during the first stages (incubation and initiation) of stress corrosion cracking (SCC) damage, leading to rupture, which can be observed on network components in service. In this framework, it is of interest to develop accelerated tests to evaluate the susceptibility to corrosion and SCC of α,β′-brasses, but the development of the accelerated tests requires a good knowledge of brass dissolution mechanisms. Abundant literature can be found for α-brass, in nitrite solutions, for example,[1–10] but not for α,β′-brasses.[11–14] The dissolution mechanisms proposed in the literature for metallic alloys are divided into two categories: selective and non-selective. Burzynska et al.[15] have shown that mechanism depends in particular on ΔE^0 (i.e., difference between the standard potentials of pure metals included as alloying elements inside the brass), on alloy composition, and on anion types present in solution. The non-selective mechanism refers to a complete dissolution of metallurgical phases of the alloys. Regarding brasses, selective mechanisms correspond to dezincification, and here two main mechanisms have also been distinguished. The first corresponds to a preferential dissolution of Zn controlled by Zn diffusion in the Cu-rich phase that has been formed. The second corresponds to a simultaneous dissolution of Zn and Cu, which turns into a preferential dissolution with re-deposition of Cu from solution.[16] Heidersbach and Verink argued that the mechanism of dezincification of α-brass was dependent on the applied potential.[17] Kumar et al.[18] demonstrated the great influence of lead on the electrochemical behavior and dezincification mechanism of brass: they showed that increase in lead content of the leaded brasses could provide an improvement in corrosion resistance only under conditions where compounds of lead get precipitated on the surface and induce passivity.

The specimens investigated in the present work were composed of α,β′-brass CuZn40Pb2 (CW617N) removed from extruded rods that were used to manufacture gas transfer valves. This specific alloy, CW617N, used principally for its good malleability and machinability (related to the Pb amount) and resistance to corrosion, is principally studied for the development of water taps.[19–22] Taking into account the lack of knowledge in the literature concerning the corrosion behavior of α,β′-brass, the present study aimed to study the electrochemical behavior of such a material. Electrochemical measurements were performed in $NaNO_3$ solutions selected on the basis of a literature review on α-brass.[23] In the literature, the solutions that are most often used are ammonia,[14,24–25] sulfuric acid,[15,26-27] and nitrite solutions[9] but, according to Fernandez et al.,[23] the nitrate ion is far more stable in low pH solution than the nitrite ion. Because the present study was a first step to develop an accelerated SCC test, nitrite ion was avoided since it was unstable in the acid solution that is expected to exist inside a stress corrosion crack. Ammonia solutions, widely used for testing brass corrosion resistance, were also excluded due to the lack of reproducibility of tests performed in this environment. Therefore, in the present work, results obtained for different pHs and nitrate ion concentrations were analyzed by comparing open circuit potential (OCP) measurements and current density vs. potential curves. Surface characterizations (Optical Microscopy and X-Ray photoelectron spectrometry) were performed to explain the electrochemical behavior observed in relation to the passive films and corrosion products formed on the sample surface depending on the potential.

Experimental

Material.— The chemical composition of the α,β′-brass CuZn40Pb2 (CW617N) is presented in Table I. Results from the inductively coupled plasma (ICP) measurements, performed on samples from extruded rods used in this study, were similar to those from the standard composition of CW617N. Optical microscope (OM) observations after abrading, polishing and etching the brass sample surface using Klemm I solution (24 g $Na_2S_2O_3$, 1 g $K_2S_2O_5$, 50 mL H_2O) for 3 minutes showed the metallurgical state of the brass.

Electrochemical tests.— Electrochemical tests were performed in $NaNO_3$ solutions (0.05 M, 0.1 M, 0.5 M, 1 M - AnalaR NORMAPUR ACS, ISO, Reag. Ph. Eur. analytical reagent). The pH of the different solutions was adjusted (11, 12, 13) by the addition of NaOH (AnalaR NORMAPUR ACS, ISO, Reag. Ph. Eur. analytical reagent).

Open Circuit Potential (OCP) measurements were performed and current density vs. potential curves were plotted with a standard device composed of a potentiostat connected to a reference electrode (Saturated Calomel Electrode), a counter electrode (platinum) and a working electrode composed of an α,β′-brass sample. The surface exposed to the electrolyte corresponded to the plane perpendicular to the extrusion direction. For all electrochemical tests, the surface area was equal to approximatively 4 cm^2. The sample surface was abraded with 4000 grit SiC paper before the experiment. After this surface

[z]E-mail: christine.blanc@ensiacet.fr

Table I. Chemical composition of the α,β′-brass CuZn40Pb2 (CW617N). Chemical composition of α and β′ phases is given.

	Inductively coupled plasma atomic emission spectroscopy		Electron microprobe			
	Extruded rod		Phase α		Phase β′	
Elements	wt %	at %	wt %	at %	wt %	at %
Zn	38.35	38.20	36.40	35.80	44.10	43.80
Al	0.008	0.019	0.008	0.02	0.01	0.03
Ni	0.051	0.057	0.12	0.13		0.10
Fe	0.205	0.239	0.26	0.30	0.08	0.09
Mn	0.004	0.005	-	-		-
Sn	0.150	0.082	0.08	0.05	0.48	0.26
Pb	1.875	0.589	0	0	0	0
Si	0.001	0.002	-	-	-	-
Cu	59.35	60.81	63.10	63.70	54.10	55.30

preparation, almost all Pb particles in the surface or near-surface were removed. Tests were performed in a beaker with 300 mL of the solution (surface/volume ratio = 1.3×10^{-2} cm^2/mL) that was open to the air and moderately stirred with a magnetic stirrer. During the tests, the beakers were placed in a thermostatically controlled water-bath maintained at 23.5 ± 2°C.

OCP values were measured for 900 s upon immersion of the working electrode and were recorded every 30 seconds. All OCP measurements were performed three times for each experimental condition to check their reproducibility. For each experimental condition, data given in the manuscript correspond to mean values calculated from the three measurements: error bars are indicated on OCP curves. Some OCP measurements were performed for longer times (6 or 24 hours) to characterize the electrochemical behavior of the brass for long times. The current density vs. potential curves were plotted, after the OCP measurements, from the last OCP value to a potential sufficient to observe the passivity breakdown at a scan rate of 0.070 mV.s^{-1}. Reproducibility of the polarization curves was also checked: three measurements were made for each experimental condition. A good reproducibility was observed; for more clarity, only one representative curve is given for each condition.

Complementary tests.— After the electrochemical tests, the samples were rinsed with distilled water and air-dried. Surface observations and analyses were performed through OM (Olympus 2000) and X-ray photoelectron spectroscopy (XPS K alpha ThermoScientific, and monochromatic excitation source A1Kα 1486.6 eV). Parameters used for OM observations coupled with a Nikon Ma2P camera were precisely controlled in order to prevent any change in the protocol of observation. White balance was performed on a Teflon specimen. In this framework, any color change can be attributed to a surface phenomenon. XPS spot size used corresponded to a 300 µm diameter area, including a high number of α and β′ grains. With the technique used, a focus on one phase was not possible due to the minimum spot size (150 µm) compared to the α,β′ grain size (20 µm). Semi-quantification and XPS peak deconvolutions after selections of the peak Binding Energy (BE) or the Kinetic Energy in the database (Table II) were made. As was done for electrochemical experiments, XPS analyses were repeated three times for each condition.

Results

Microstructure.— The metallurgical state of the brass corresponded to that of the center of a 65 mm diameter extruded rod (Figure 1). The α phase (64 at. % Cu, 36 at. % Zn, Table I) was enveloped in β′ phase (55 at. % Cu, 45 at. % Zn, Table I), which is in agreement with the solidification processes expected for CuZn40Pb2 alloys. A transverse section of the rod was characterized by equiaxed grains (α and β′ phase) with an average size of 24 µm in diameter for the α phase and 20 µm for the β′ phase. Observations of the longitudinal sections of the rod showed a texturation of the β′ grains (their size varied from 20 µm to 120 µm in the longitudinal direction compared to 20 µm in the transverse direction). Moreover, the α grains distribution in the longitudinal section was heterogeneous: α grains had preferentially germinated at the β′ grain boundaries, leading to a specific chaining of β′ and α phases. Because lead is insoluble in Cu-Zn alloys, lead-rich micro-particles were also observed depending on the surface preparation; they were finely dispersed in the alloy but mainly present at the α,β′-interphases and in the β′ phase.

Electrochemical behavior of α,β′-brass CuZn40Pb2.— The electrochemical behavior of α,β′-brass CuZn40Pb2 during immersion in different $NaNO_3$ solutions is presented as OCP vs. time curves (Figure 2). For the major part, these curves were plotted during 15 minutes upon immersion of the samples in the electrolyte for various chemical conditions, i.e. different pH values for a 0.5 M $NaNO_3$ solution (Figure 2a) and different nitrate ion concentrations for a pH 11 solution (Figure 2b). For all the chosen pH and the nitrate ion concentration (Figures 2a and 2b), the OCP first increased rapidly (except for pH 13, Figure 2a) and then tended to stabilize, which could be associated with passivation or pseudo passivation of the exposed surface. The results showed that the pH (Figure 2a) significantly influenced the OCP measurements. In the first 400 seconds, the variation of OCP vs. time was faster when the pH decreased. This effect was markedly visible for pH 13 with OCP values quite stable during the first 420 s, followed by a strong increase of the OCP between 420 and 600 s and then a stabilization. Furthermore, the OCP value was stabilized at −0.270 ± 0.007 V/SCE for a pH of 13 whereas for a pH equal to 12

Table II. Selected binding energies (BE) or Auger kinetic energies (KE) in eV for the characteristic peaks.

Name	Peak BE (eV)	Reference (eV)
Zn $2p_{3/2}$ /Zn	1021.5	C 1s 285.0
Zn $2p_{3/2}$/ZnO	1022.7	
Zn 3s	140.4	
Cu $2p_{3/2}$/Cu	932.4	C 1s 285.0
Cu $2p_{3/2}$/Cu_2O	932.4	
Cu $2p_{3/2}$/CuO	933.5	
Cu $2p_{3/2}$/$Cu(OH)_2$	935.2	
Pb $4f_{7/2}$/Pb	136.5	C 1s 285.0
Pb $4f_{7/2}$/PbO	138.2	
Pb $4f_{7/2}$/$Pb(OH)_2$	138.7	
	Peak KE (eV)	
Cu $L_3M_{45}M_{45}$/Cu	918.8	C 1s 285.0
Cu $L_3M_{45}M_{45}$/CuO	918.0	
Cu $L_3M_{45}M_{45}$/Cu_2O	916.8	
Cu L_3VV	914.8 & 921.5	

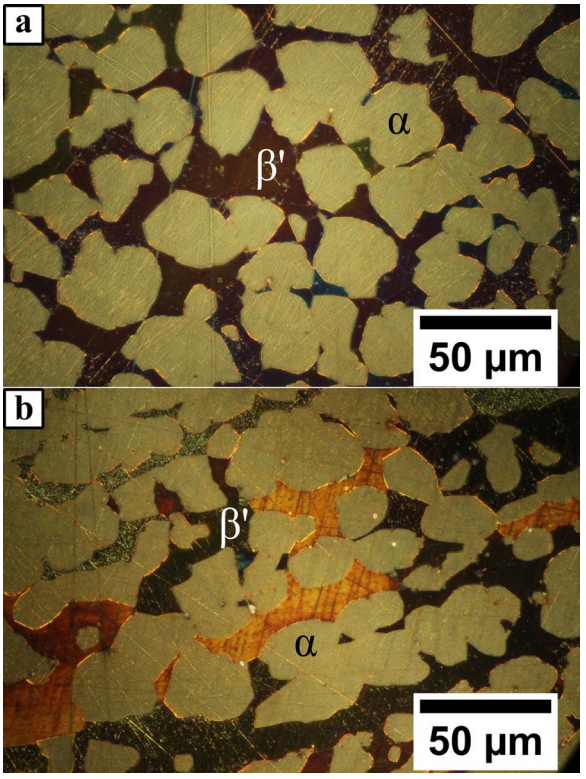

Figure 1. Optical microscope observations of the α,β′-brass CuZn40Pb2 (CW617N). The sample was observed after polishing followed by Klemm I etching. (a) transverse section (b) longitudinal section.

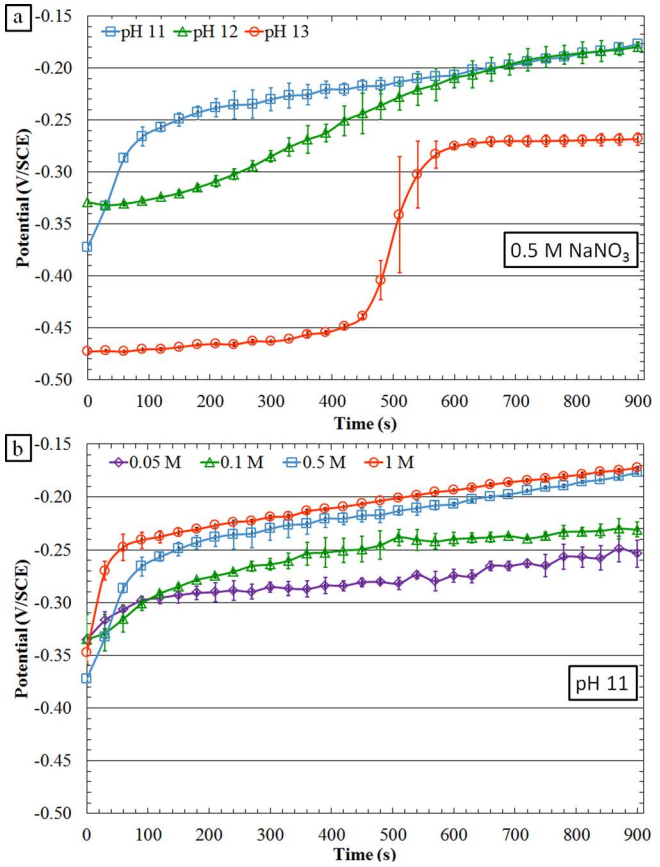

Figure 2. OCP vs. time of the α,β′ brass CuZn40Pb2 (a) at various pH, in a 0.5 M $NaNO_3$ solution (b) at various $NaNO_3$ concentrations, pH 11.

and 11, the OCP reached a value of approximately -0.178 ± 0.005 V/SCE after 900 s in solution but that was not totally stabilized, as confirmed by longer measurements. OCP measurements performed for longer times, i.e. 6 hours, showed that OCP values stabilized at -0.07 ± 0.02 V/SCE, -0.15 ± 0.02 V/SCE and -0.22 ± 0.01 V/SCE for pH 11, 12 and 13, respectively. The results showed a better corrosion behavior for low pH values assuming that the OCP increase was caused by passivation and not by an increase in the cathodic reaction rate. The results were probably correlated to changes occurring on the sample surface that were strongly dependent on pH, for example modification of the chemical composition of the passive layer. Figure 2b shows the influence of the nitrate ion concentration on OCP values for a pH 11 solution. The effect of the nitrate ion concentration was less significant than that of the pH. Globally, all curves presented the same shape with a rapid increase of the OCP in the first part of the immersion. The OCP value reached after 15 minutes in solution increased with the nitrate ion concentration with mean values from -0.25 ± 0.01 V/SCE to -0.172 ± 0.005 V/SCE for nitrate concentration in the range [0.05 M; 1 M]; however longer tests showed that the OCP values were almost independent of the nitrate ion concentration. For all nitrate concentrations, OCP stabilized at -0.07 ± 0.02 V/SCE after 6 h and at -0.072 ± 0.006 V/SCE after 24 h (mean value and standard deviation calculated using data for all nitrate concentrations with 3 OCP values for each concentration, i.e. 12 OCP values). Small differences in the OCP vs. time for the four nitrate ion concentrations might be related to the O_2 availability in solution affected by the nitrate ion concentration.

The anodic behavior of the material in nitrate solutions, evaluated through current density vs. potential curves plotted in the anodic domain after 15 minutes at OCP, is shown in Figure 3. Globally, all curves presented a similar shape: after the corrosion potential,

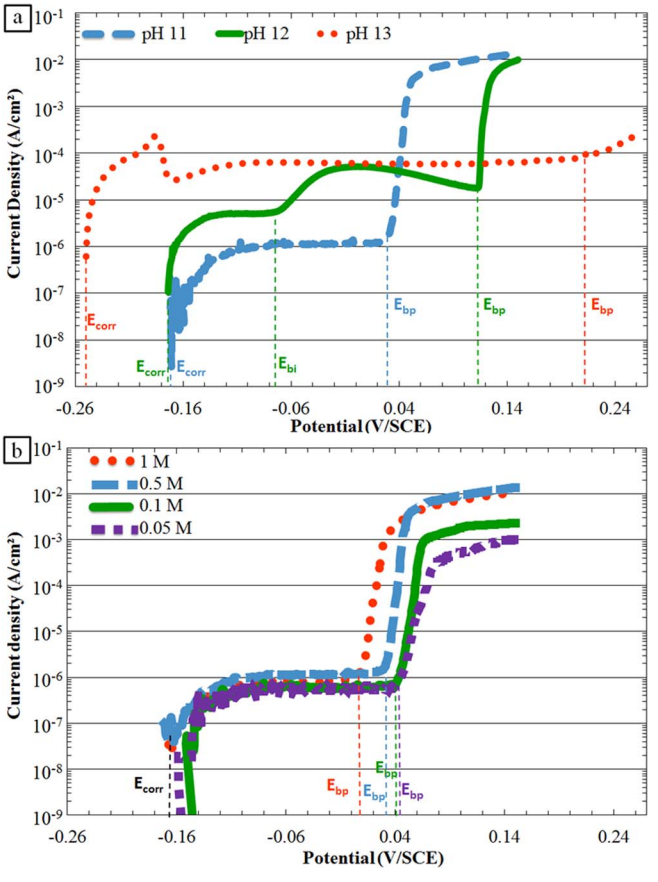

Figure 3. Current density vs. potential curves for the α,β′ brass CuZn40Pb2 (a) at various pHs, 0.5 M $NaNO_3$ (b) at various nitrate ion concentrations, pH 11.

E_{corr}, a passivity or pseudo-passivity plateau was observed, followed by a breakdown potential, E_{bp}, and finally a strong increase of the current densities corresponding to the passivity or pseudo passivity breakdown. Figure 3a shows the influence of the pH on the current density vs. potential curves for a 0.5 M $NaNO_3$ solution. The shift of the OCP toward more negative values when the pH value increased, as shown in Figure 2a, was clearly evidenced on the current density vs. potential curves with the shift of E_{corr}. Furthermore, a significant influence of the pH was observed on the current densities and on the values of the breakdown potential, E_{bp}. At pH 11, a passivity plateau was observed that was characterized by low current densities approximately 10^{-6} A.cm^{-2} before E_{bp}. For a pH 12 solution, an intermediate breakdown potential, E_{bi}, was evidenced: E_{corr} was first followed by a passivity plateau at higher current densities than for pH 11, i.e., approximately 5×10^{-6} A.cm^{-2}; then, after E_{bi}, a pseudo-passivity plateau characterized by current densities approximately 6×10^{-5} A.cm^{-2} was observed before the breakdown potential E_{bp}. At pH 13, only the pseudo-passivity plateau was observed before E_{bp} with current density values similar to those values for pH 12. Both the shift of E_{corr} toward more negative values and the increase of the anodic current densities when the pH increased were consistent with a decrease of the corrosion resistance of the α,β′-brass when the pH increased. On the contrary, concerning the breakdown of the passivity or the pseudo passivity, observations showed that an increase in the pH shifted the breakdown potential, E_{bp}, toward more positive potentials leading to an increase of the passive or pseudo-passive range. Similar to the OCP results (Figure 2b), the effect of nitrate ion concentration on the current density vs. potential curves was studied for a pH 11 solution (Figure 3b). The results showed that a variation in nitrate ion concentration did not significantly affect the current density vs. potential curves. It had no effect on the current densities of the passivity stage; however, a decrease in the nitrate ion concentration led to a small shift of the breakdown potential, E_{bp}, toward more positive potentials as observed for an increase in pH. Additional experiments showed that, in adjusted pH solutions without $NaNO_3$, the passivity breakdown was not observed at pH 11 and pH 12, whereas the current densities during the passivity stages were similar to those measured in the presence of nitrate ions. As stated by Fernandez et al.,[23] for α-brass, NO_3^- could play a role in the corrosion mechanism observed after the passivity breakdown.

Characterization of the sample surface after electrochemical tests.— Electrochemical tests were complemented further by OM observations and XPS analyses. Because the pH was found to have the major influence on electrochemical results, attention was paid to modification of the surface chemical composition depending on the pH of the electrolyte. Experiments were performed in a 0.5 M $NaNO_3$ solution at pH 11 and 12. Surface analyses were performed for samples after interrupted polarization tests in order to get a better insight on the electrochemical behavior observed for the α,β′ brass.

To characterize the corrosion behavior of the α,β′ brass CuZn40Pb2 at the corrosion potential, surface analyses were first performed for samples after 15 minutes at OCP. Comparison of OM observations before immersion (Figure 4a) and after 15 minutes at OCP in a 0.5 M $NaNO_3$ solution at pH 11 (Figure 4b) showed an orange discoloration of the β′ phase after immersion while no change was observed for the α phase. This discoloration became more pronounced after 15 minutes at OCP in a 0.5 M $NaNO_3$ solution at pH 12 (Figure 4c). These observations were assumed to be mainly due to the formation of a passive or pseudo passive layer, in agreement with the passive or pseudo passive region observed in the current density vs. potential curves (Figure 3), and the evolution in its chemical composition as well as dezincification process of the sample surface, in particular of the β′ phase. XPS analyses were performed to corroborate this assumption. Figure 5 shows general XPS spectra obtained for an as received sample (before exposure to nitrate solutions) and for a sample after a 15 minute immersion at the OCP in a pH 11 solution. For the as received sample, Zn and Cu characteristic peaks were detected, as well as O and C peaks. No significant Pb signal was detected probably

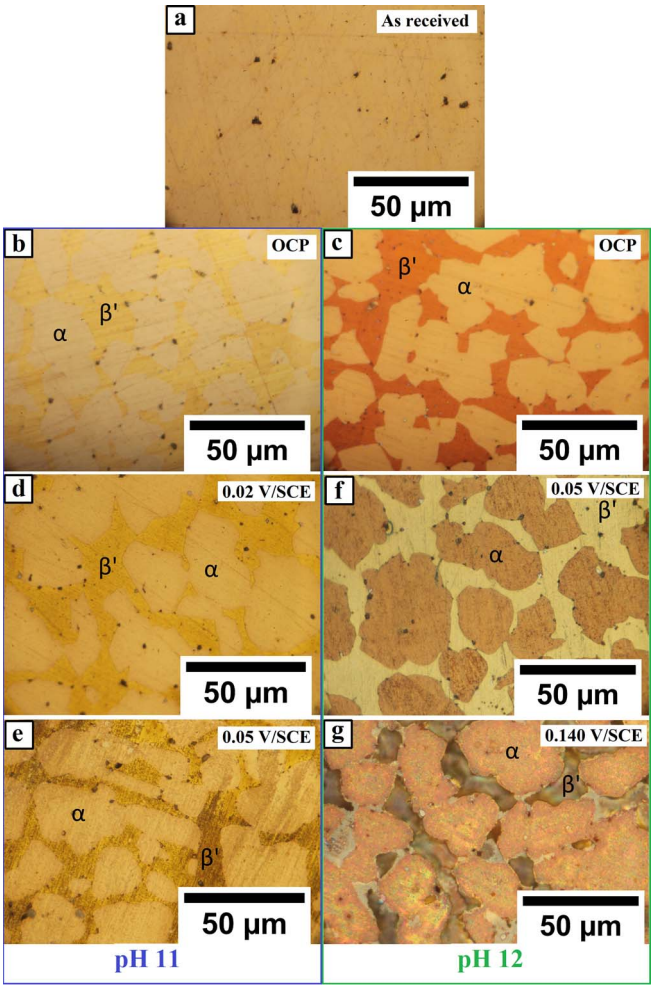

Figure 4. Optical microscope observations of the α,β′ brass CuZn40Pb2 sample surface. Before immersion (a). After 15 minutes at OCP in a 0.5 M $NaNO_3$ solution at pH 11 (b) and at pH 12 (c). Figures (d) to (g) correspond to optical microscope observations of the α,β′ brass CuZn40Pb2 after interrupted anodic polarization tests in a 0.5 M $NaNO_3$ solution (d) before the passivity breakdown (0.02 V.SCE), pH 11 (e) after the passivity breakdown (0.05 V.SCE), pH 11 (f) before the pseudo-passivity breakdown (0.05 V.SCE), pH 12 (g) after the pseudo-passivity breakdown (0.14 V.SCE), pH 12.

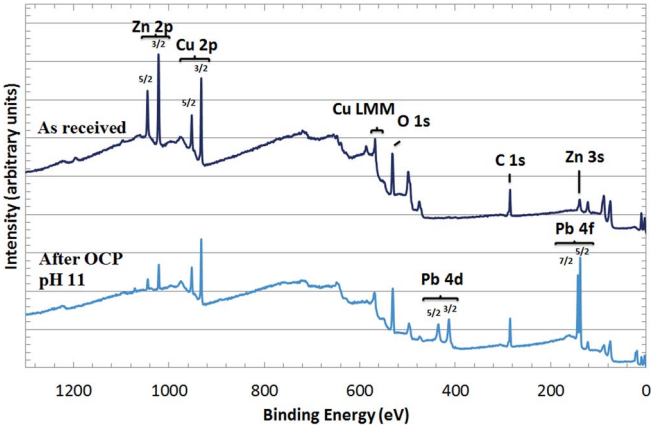

Figure 5. General XPS spectra and identification of the characteristic peaks on α,β′ brass CuZn40Pb2. Spectra are plotted for a sample before exposure to nitrate solutions (labeled as received) and for a sample after a 15 minute immersion at OCP in a pH 11 solution (0.5 M $NaNO_3$).

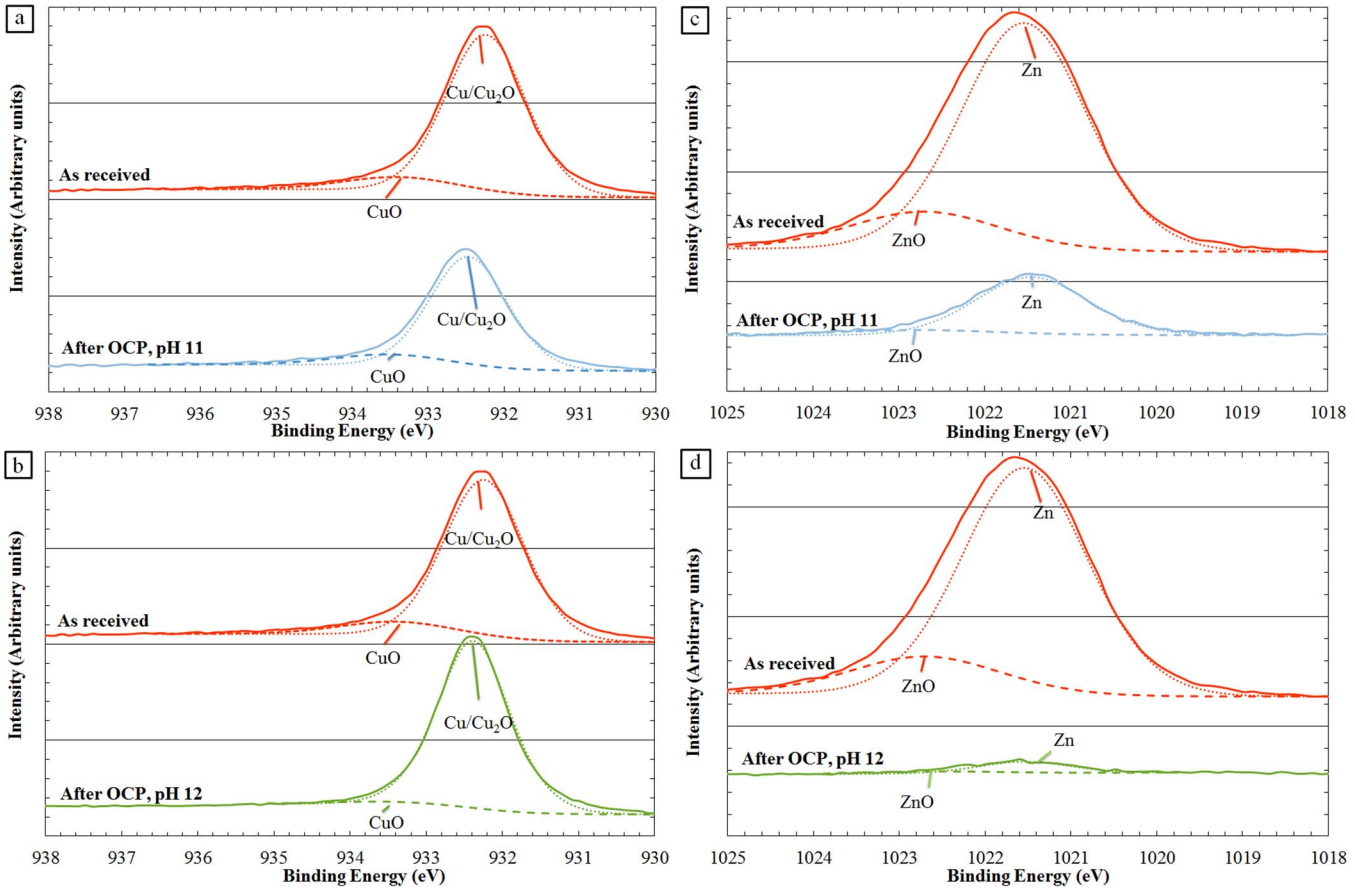

Figure 6. XPS analyses of α,β′-brass CuZn40Pb2 performed after a 15 minute immersion at the OCP in a 0.5 M $NaNO_3$ solution. Focus on (a) and (b) Cu 2p3/2 peaks, (c) and (d) Zn 2p3/2 peaks. Figures (a) and (c) correspond to a pH 11 solution. Figures (b) and (d) correspond to a pH 12 solution. On each figure, XPS analyses for an as received sample are reported.

due to the removal of the Pb particles during polishing. Attention was paid to the Cu $2p_{3/2}$ and Zn $2p_{3/2}$ peaks. For the as received sample, the intensity of the Cu $2p_{3/2}$ (Figure 5, Figures 6a and 6b) and Zn $2p_{3/2}$ (Figure 5, Figures 6c and 6d) peaks were strong. Deconvolution of these peaks, as well as that of the Auger Cu peak (Figure 7), showed that the surface of the as received sample was covered by a passive film mainly composed of Cu_2O and ZnO (Table III). The signals of metallic species were strong showing that this film was thin. After a 15 minutes immersion at OCP in the pH 11 solution, a significant decrease of the Zn $2p_{3/2}$ peak was evidenced (Figures 5 and 6c). This was confirmed by XPS semi-quantitative analysis of the samples (Figure 8a) with a stronger Cu/Zn ratio after OCP than for the as received sample. The results thus corroborated the dezincification hypothesis; they also showed the presence of a significant amount, i.e. about 27 at. %, of Pb in the passive layer (Figures 8a and 9a). The passive layer was mainly composed of Cu_2O with a very low amount

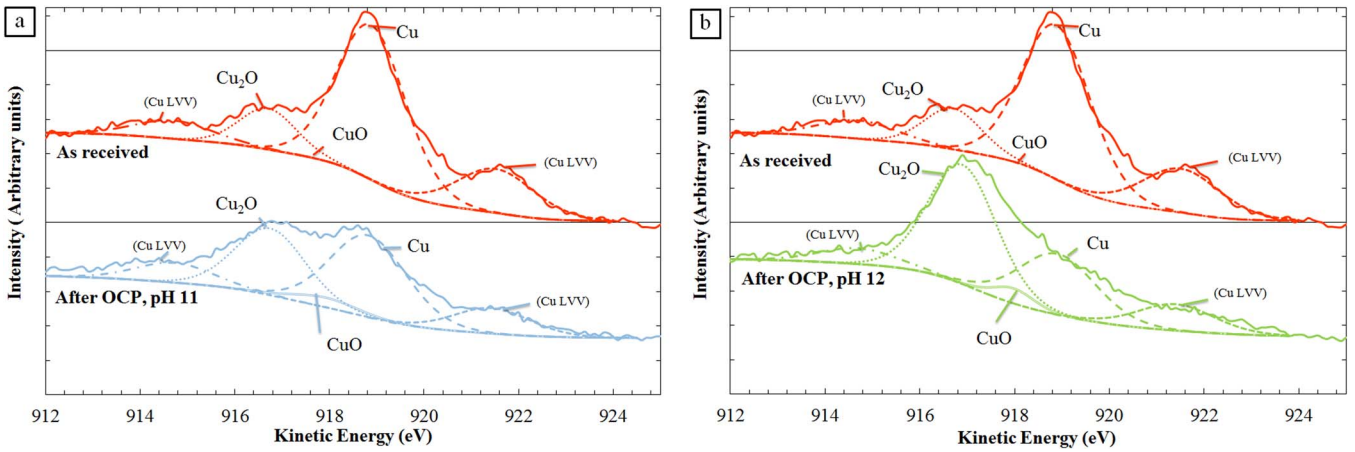

Figure 7. XPS analyses of the α,β′-brass CuZn40Pb2 performed after a 15 minute immersion at the OCP in a 0.5 M $NaNO_3$ solution: focus on the Cu LMM Auger peaks (a) for a pH 11 solution and (b) for a pH 12 solution. Results for an as received sample are reported for comparison.

Table III. Synthesis of electrochemical results and XPS semi-quantification.

	pH 11				pH 12		
E_{corr} (from I-E curves) (V/SCE)	−0.17				−0.17		
$I_{passivity}/I_{pseudo\text{-}passivity}$ ($A.cm^{-2}$)	10^{-6}/—				$5.10^{-6}/6.10^{-5}$		
E_{bp} (V/SCE)	0.03				0.115		
at % (Shirley Background)	As received	After OCP	Before passivity breakdown 0.02 V/SCE	After passivity breakdown 0.05 V/SCE	After OCP	Before pseudo-passivity breakdown 0.05 V/SCE	After pseudo-passivity breakdown 0.14 V/SCE
Zn $2p_{3/2}$/Zn	41 ± 5	11 ± 3	11 ± 3	11 ± 3	2.1 ± 1	6.1 ± 2	4.1 ± 1
Zn $2p_{3/2}$/ZnO	8.0 ± 2	1.5 ± 0.5	<1	<1	<1	3.0 ± 1	<1
Cu $2p_{3/2}$/Cu_2O	30 ± 4	24 ± 4	29 ± 4	16 ± 3	41 ± 5	5.2 ± 2	44 ± 5
Cu $2p_{3/2}$/CuO	3.4 ± 1	3.4 ± 1	2.6 ± 1	10 ± 3	1 ± 0.4	19 ± 3	4 ± 1
Cu $2p_{3/2}$/$Cu(OH)_2$	-	-	-	-	-	16 ± 2	-
Pb $4f_{7/2}$/$Pb(OH)_2$	-	1.8 ± 1	-	-	<1	<1	-
Pb $4f_{7/2}$/PbO	-	25 ± 4	13 ± 3	23 ± 4	22 ± 4	<1	7.4 ± 2
O 1s/O-metal	18 ± 3	33 ± 4	44 ± 10	38 ± 4	33 ± 4	49 ± 5	39 ± 4
Cu $L_3M_{45}M_{45}$/Cu_2O	8 ± 3	6 ± 3	23 ± 6	10 ± 4	26 ± 5	2.1 ± 2	38 ± 10
Cu $L_3M_{45}M_{45}$/Cu	22 ± 4	18 ± 4	6 ± 4	6 ± 3	15 ± 4	3.1 ± 2	6 ± 3

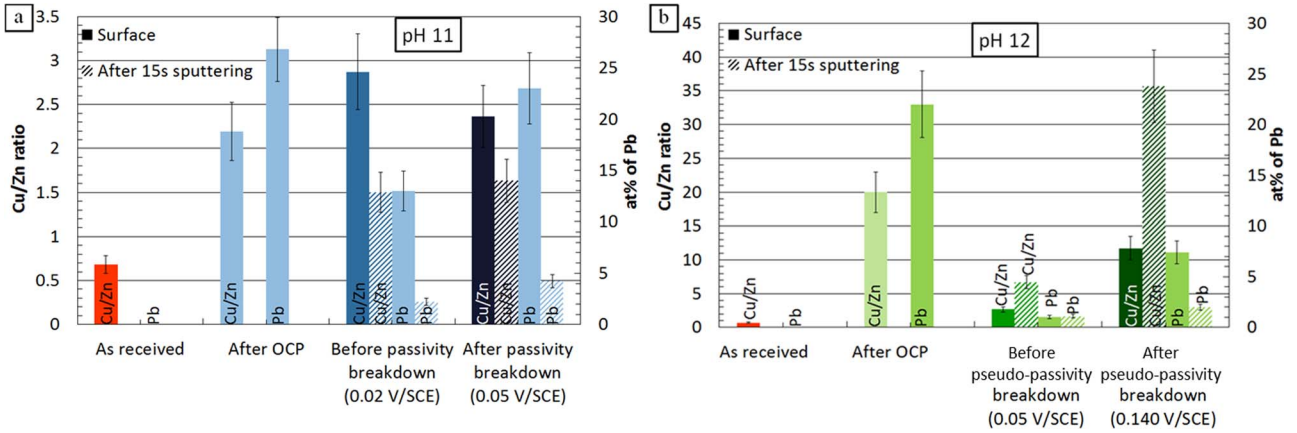

Figure 8. Cu/Zn ratio and Pb amount for the α,β′ brass CuZn40Pb2 after immersion at the OCP and after interrupted anodic polarization tests in a 0.5 M $NaNO_3$ solution (a) at pH 11 (b) at pH 12. The results of a sample before exposure (labeled as received) are reported for comparison.

of ZnO but a significant amount of Pb oxides (Figure 6a, Figure 6c, Figure 7a, Figure 8a, Figure 9a and Table III). When the sample was maintained at OCP in a pH 12 solution, the intensity of the Zn $2p_{3/2}$ peak was significantly reduced (Figure 6d) by comparison to the pH 11 solution (Figure 6c) with a markedly higher Cu/Zn ratio after OCP at pH 12 (Figure 8b) compared to pH 11 (Figure 8a). The results thus showed that the dezincification process was markedly increased when the pH increased. After immersion at OCP in pH 12 solutions, the passive layer was mainly composed of Cu_2O (Figures 6b and 7b) with Zn being significantly depleted at the surface (Table III).

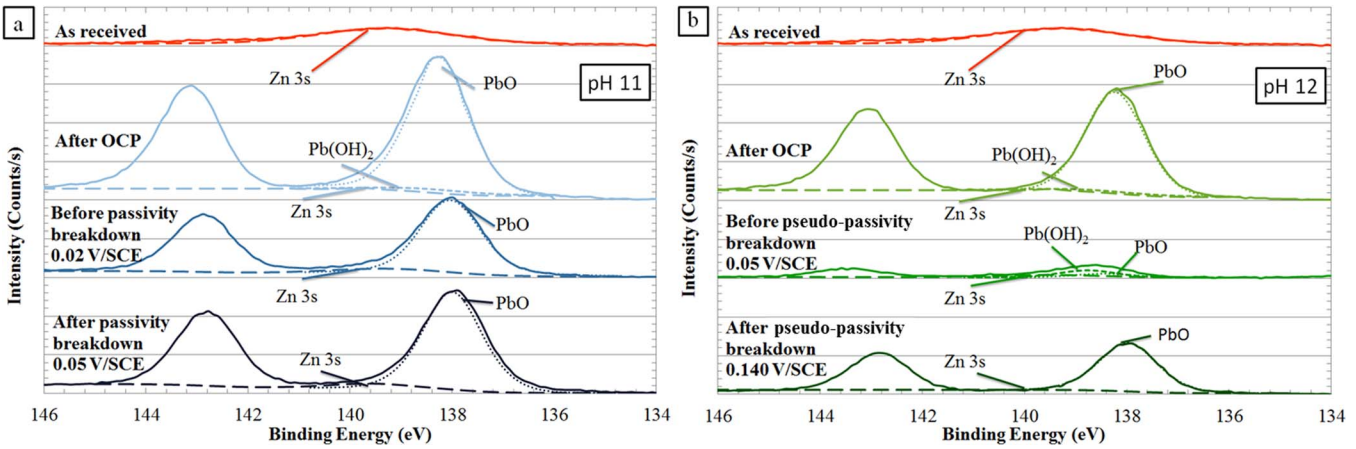

Figure 9. XPS analyses of the α,β′-brass CuZn40Pb2: focus on the Pb $4f_{7/2}$ peak. Results are given after OCP and after interrupted polarization tests in a 0.5 M $NaNO_3$ solution (a) for a pH 11 solution (b) for a pH 12 solution. On each figure, results for an as received sample are reported for comparison.

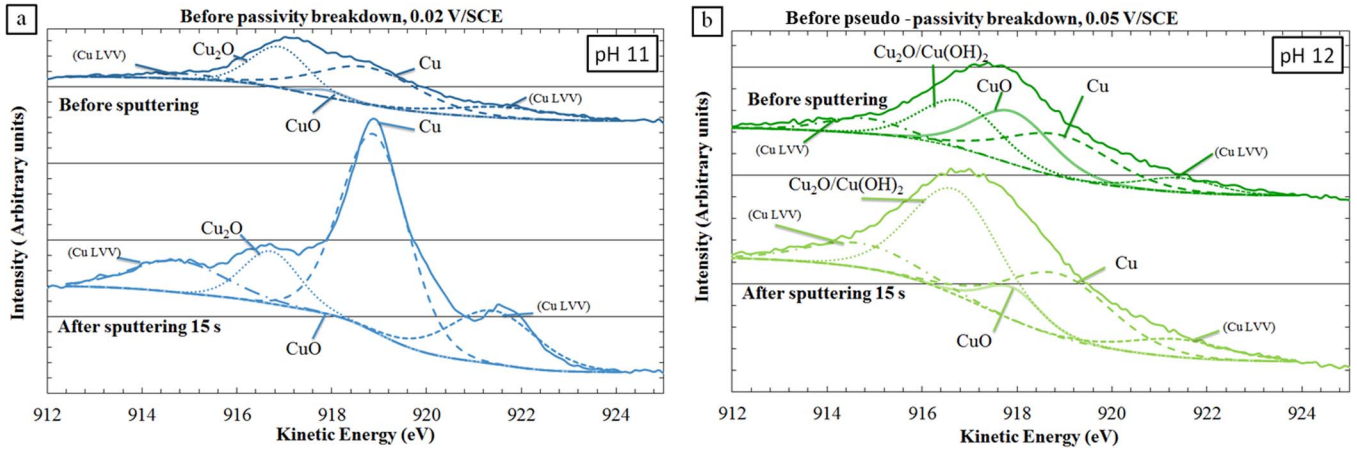

Figure 10. XPS analyses of the α,β′-brass CuZn40Pb2 after interrupted polarization tests until a potential before the passivity or pseudo-passivity breakdown. Focus on Cu LMM peaks for (a) a pH 11 solution and (b) a pH 12 solution. For each graph, results are given before and after 15 s of argon ion sputtering: a few hundred nanometers of the surface was removed.

About 23 at. % Pb was also present in the passive layer, as oxides or hydroxides (Figures 8b and 9b, Table III). Comparison of the spectra (Figures 7a and 7b) allowed a qualitative assessment of the passive layer thickness. After OCP at pH 11 (Figure 7a), the signal of metallic Cu was similar to the Cu_2O signal while, for pH 12 (Figure 7b), the Cu_2O signal seemed stronger compared to the metallic Cu signal suggesting that the passive film formed at pH 12 was thicker than that formed at pH 11.

Concerning the corrosion behavior of the brass under anodic polarization, OM surface observations and XPS chemical analyses were performed after interrupted polarization tests. Selected arrest potentials for analyses were chosen at points before and after the passivity or pseudo-passivity breakdown characterized by the breakdown potential, E_{bp}, as identified on the current density vs. potential curves (Figure 3). At pH 11, E_{bp} was equal to 0.030 ± 0.005 V/SCE (Figure 3a); the selected arrest potentials for analyses were chosen at 0.02 V/SCE and 0.05 V/SCE for characterization before and after the passivity breakdown respectively. At pH 12, E_{bp} was equal to 0.114 ± 0.005 V/SCE (Figure 3a); the selected arrest potentials for analyses were chosen at 0.05 V/SCE and 0.14 V/SCE respectively. Concerning the potential of the passivity or pseudo-passivity plateau, due to the differences in the current density values, the arrest potentials were chosen to be close to the end of the plateau. For the potential after the passivity breakdown, the arrest potentials were chosen to correspond to a similar current density of 8×10^{-3} A/cm^2.

At pH 11, during the passivity stage, OM observations (Figure 4d) did not show a significant difference compared to the results obtained after OCP exposure (Figure 4b), which was confirmed by XPS analyses (Table III) with no significant chemical change of the surface for Cu and Zn amounts (Figure 8a). The formation of a Cu_2O layer was revealed (Figure 10a) and no more dezincification had occurred. Pb oxides were still detected (Figure 9a) but with a significantly lower amount, i.e. only 13 at. %. Cu in metallic form was still identifiable (Figure 10a) suggesting that the passive layer should be thin. The thickness of the layer was assessed by a new analysis after a short period of argon ion sputtering (15 s), the removed surface being estimated about a few hundred nanometers. The results revealed a strong signal for metallic Cu (Figure 10a) and a lower Cu/Zn ratio (Figure 8a) corresponding to a less dezincified layer with a very low Pb amount. After the breakdown potential, OM observations (Figure 4e) showed that the β′ phase started to dissolve locally while the α phase appeared to remain stable. XPS analyses (Table III and Figure 8a) showed a Pb amount similar to that after OCP exposure, with Pb oxides present in the passive layer (Figure 9a) but no significant differences concerning the major elements, i.e., Cu and Zn, compared to the results on the passivity plateau (Figure 8a). This was probably because the breakdown of the passivity corresponded to local corrosion phenomena on the β′ phase. Concerning results obtained at pH 12, before the end of the pseudo-passivity stage, OM observations (Figure 4f) showed an inversion in color between the α and the β′ phases. A new surface layer seemed to be formed on the α phase. XPS analyses (Figure 11) showed the formation, on the sample surface, of a layer mainly composed of Cu_2O, CuO and $Cu(OH)_2$; Table III showed that ZnO participated in the formation of this surface layer as confirmed by the relatively low Cu/Zn ratio (Figure 8b) while, after OCP exposure, Zn was depleted at the surface. After 15 s of argon ion sputtering, the Zn signal was reduced (Figure 8b); however, the signals of copper oxides and hydroxides were still strong (Figure 10b) suggesting that the pseudo-passive layer formed at pH 12 was thicker than that formed at pH 11 (Figure 10a). It was assumed that this layer was constituted of a ZnO-rich external layer covering a Zn-poor internal layer. The Pb amount was very low (Figures 8b and 9b). After the breakdown potential, OM observations showed that the β' phase was considerably dissolved (Figure 4g) while a layer remained on the α phase. XPS analyses (Table III, Figure 11) revealed some significant changes in the chemical composition of the surface layer. CuO and $Cu(OH)_2$ signals were not observed while Cu_2O was still detected. Concerning Zn, after the pseudo-passivity breakdown, the Zn signal was significantly reduced compared to Zn signal before pseudo-passivity breakdown but remained slightly higher than after OCP (Table III and Figure 8b); results obtained after 15 s of argon ion sputtering suggested that the corrosion phenomena extended in depth. The very low amount of Zn in the surface layer might be correlated to the strong dissolution of the β' phase. As previously stated, the immersion of the α,β′ brass at the OCP in a pH 12 solution led to a dezincification phenomenon stronger than at pH 11. When the brass was polarized at potentials corresponding with the pseudo-passivity, a thick surface layer formed characterized by an incorporation of Zn as ZnO into the external surface layer covering a Zn-poor internal surface layer. When the sample was polarized at a higher potential, after the pseudo-passivity breakdown, this thick surface layer was removed and its chemical composition strongly evolved. Complete dissolution of the β′ phase was observed. Pb oxides were incorporated into the layer, with the Pb amount reaching 7 at. % (Figure 9b).

Discussion

Immersion of the α,β′-brass CuZn40Pb2 in basic solutions of sodium nitrate (pH 11, 12 and 13) at the OCP led to a spontaneous surface dezincification. This occurred simultaneously with the formation of a passive or pseudo-passive oxide layer that was identified by XPS analyses. The results showed that this layer was mainly composed of copper oxide although, when considering the proportion of lead oxide determined by a XPS semi-quantitative analysis, PbO could play

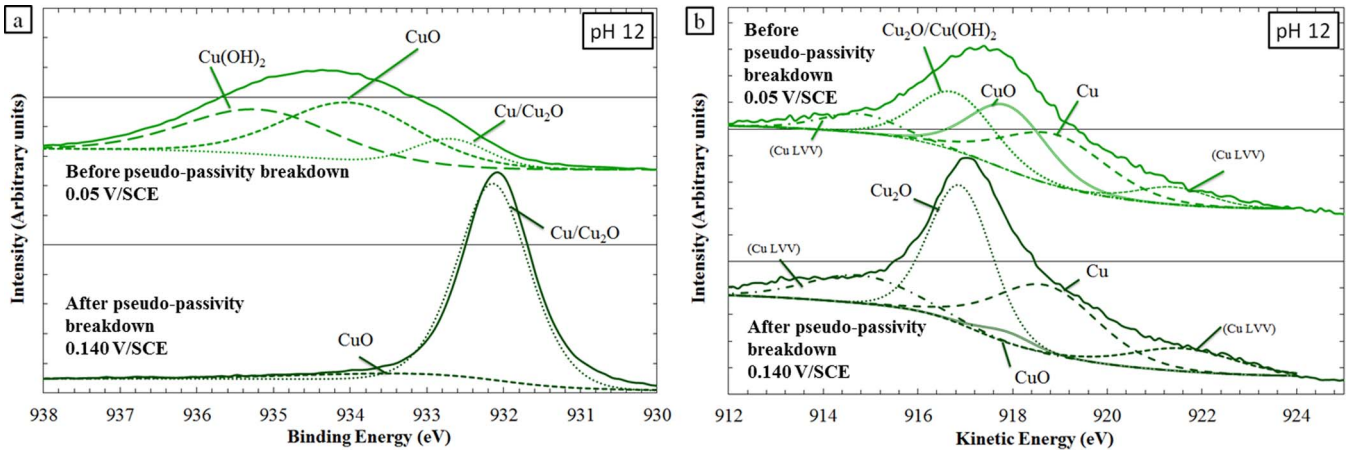

Figure 11. XPS analyses of the α,β′-brass CuZn40Pb2 after electrochemical tests in a 0.5 M $NaNO_3$ solution (pH 12). Focus on (a) Cu 2p3/2 peaks and (b) Cu LMM peaks. On each figure, XPS analyses were performed for samples after interrupted polarization tests until the potentials before and after the pseudo-passivity breakdown.

a significant role in the passive or pseudo passive layer properties. After polarization in the anodic domain, no more dezincification was observed for a pH 11 solution and, after the passivity breakdown, local corrosion of β′ phase was observed; for pH 12, complete dissolution of the β′ phase occurred after the pseudo-passivity breakdown. The results showed that the electrochemical behavior of the α,β′-brass CuZn40Pb2 in basic solutions of sodium nitrate depended both on pH and the applied potential but the influence of Pb had to be taken into account.

Influence of the applied potential on the dissolution mechanisms.— At the microstructural scale, OM observations performed for samples maintained at the OCP indicated that the α phase was relatively stable in the nitrate solutions compared to the β′ phase, for which the chemical composition strongly evolved due to complex dissolution mechanisms, for both pH 11 and pH 12 solutions. Dezincification of the β′ phase was clearly evidenced with an orange discoloration of this phase (Figures 4b and 4c) correlated to Zn preferential dissolution as confirmed by XPS analyses (Figures 8a and 8b). The results were in agreement with the work of Pickering et al.[28–30] These authors showed that the selective dissolution of Zn occurred from the alloy surface at the steady state condition. The galvanic coupling between the two phases probably acted according to the mechanism proposed by Assouli et al.[31] Small electrochemical cells could exist at the microstructural scale with the α phase, which contains more copper than the β′ phase, being more noble than the β′ phase and acting as the cathode while the β′ phase was the anode. Therefore, passivation of the α phase could occur with the formation of a copper oxide layer. Concerning the β′ phase, an initial dezincification process should be necessary to achieve a surface that was more noble and susceptible to passivation, leading to the formation of a copper/lead oxide layer. The presence of lead particles at the interface between α and β′ phases and inside the β′ phase should affect the galvanic coupling as suggested by Kumar et al.[18] These particles were removed after polishing on the extreme surface (as received sample in Figure 5) but, after exposure to the electrolyte, due to electrochemical processes, new lead-rich particles were exposed to the electrolyte. However, Pickering et al.[28–30] showed that, at a high electrode potential, dissolution of Zn was enhanced because of the simultaneous dissolution of Cu and Zn from alloy surface. Heidersbach and Verink proposed that, for low potentials, preferential dissolution of Zn occurred while, for higher potentials, both copper and Zn dissolved with or without copper re-deposition depending on the potential value.[17] The results obtained in the present work corroborated these assumptions: for a pH 11 solution, no more dezincification was observed during anodic polarization compared to the OCP results (Figure 8a) and corrosion phenomena were essentially observed on the β′ phase, which was more reactive than the α phase due to its higher Zn amount. For a pH 12 solution, before the pseudo-passivity breakdown, Zn was incorporated into the pseudo-passive layer (Figure 8b). Because XPS analyses only allowed a global analysis of the surface, it was difficult to distinguish between the electrochemical processes occurring on the α phase and on the β′ phase. OM observations performed after the pseudo-passivity breakdown clearly showed that only the β′ phase was corroded while the α phase remained passive. It was assumed that, before the pseudo-passivity breakdown, both copper and Zn dissolved from the β′ phase while the passive film formed on the α phase might contain both copper and Zn species. This could explain that the Zn amount (9 at. %) measured before the pseudo-passivity breakdown (Table III) was higher than after OCP (2 at. %). After the pseudo-passivity breakdown, a complete dissolution of the β′ phase was evidenced, which might explain the lower Zn amount measured on the surface layer (about 4 at. %) compared to that measured before the pseudo-passivity breakdown (Table III). However, the Cu/Zn ratio after the pseudo-passivity breakdown remained lower than after OCP corroborating that, for this range of potential, the corrosion mechanism of the α,β′-brass, and in particular the dissolution of β′ phase, involved both copper and Zn dissolution more than a dezincification process.

Influence of pH and role of Pb.— OCP values were found to decrease with an increase in pH (Figure 2a) which was clearly evidenced after long immersion times. This was in agreement with previous studies on α-brass.[23] The differences in the chemical composition and structure of the surface layer depended on the pH, with a higher dezincification process, for pH 12 solutions compared to pH 11 solutions, leading to a more porous structure of the brass surface as suggested by Pickering et al.[28–30] Concerning the selective dissolution of the Zn present in the β′ phase, the Pourbaix diagram for Zn shows that Zn stability decreases when the pH increases. $Zn(OH)_2$ is the most stable species until pH 10. Beyond that, $HZnO_2^-$ and ZnO_2^{2-} are the thermodynamically stable species, which could explain the corrosion that the β′ phase undergoes in solutions over the range of pH that was tested. The level of the β′ phase dezincification as a function of pH may be associated with the propensity of the Zn dissolution in this phase. Dezincification was faster as the pH increased, but, for immersion at OCP, dezincification did not affect the material in the bulk as suggested by XPS analyses. This was in agreement with the stabilization of the OCP (Figure 2). This could be due to the formation of a copper-rich surface layer that is stable in this pH range. As suggested by Pickering et al., a dense layer of the more noble metal should prevent further anodic dissolution of the less noble metal.[28–30] The range of pH corresponded to the stability of Cu, Cu_2O and CuO (for higher

potentials) according to Pourbaix diagram of pure copper. These data could be easily extended to brass to explain the formation of the Cu_2O passive layer in this range of pH for the α phase and for the β′ phase after the initial stage of surface dezincification (Table III). However, the results showed that the influence of Pb could not be neglected because, for both pHs, a large amount of Pb oxides was detected in the passive layer (Figure 8). This was in agreement with the results of Korshin et al.[32] who showed the presence of Pb-rich corrosion products on brass surface after exposure to a corrosive environment by using SEM and X-ray diffraction experiments. Kumar et al.[18] corroborated the results with SEM observations of Pb-rich corrosion products on brass after exposure to NaCl solutions. They proposed that lead could explain an increase in the corrosion current of brass due to galvanic coupling between Pb particles and the rest of the alloy; at the same time, they showed that the precipitation of lead-based compounds on the surface of the brass, for potentials higher than the corrosion potential, decreases the extent of corrosion attack. In the present work, semi-quantitative XPS results showed that Pb oxides were present in the passive layer at the OCP. The amount of Pb oxides inside the passive layer was similar for both pH 11 and 12. Therefore, at the OCP, the presence of Pb oxides in the passive layer probably influenced the electrochemical behavior of the brass but, the variations observed with the pH probably reflected the variations concerning the copper oxide layer stability and growth rate and the propensity of the Zn dissolution that was dependent upon the pH. Concerning the behavior of the brass under anodic polarization (Figure 3a), the pH effect was also strong. At low pH (11), a passivity stage was observed whereas at higher pH (12 or 13), only a pseudo-passivity phenomenon was observed. This is in agreement with the results obtained by Fernandez et al.[23] who showed that the passivity current density increased when the pH increased for a Cu-37Zn alloy in 1M $NaNO_3$. With increasing pH value, the passive layer formed should be considered as less efficient. At pH 11, Pb oxides were detected in the passive layer formed at anodic potentials corresponding to the passivity plateau. They were also detected after the passivity breakdown (Figures 8a and 9a). It is of interest to recall at this stage that lead particles were mainly present inside the β′ phase and, for pH 11, only local corrosion phenomena were observed on the β′ phase after the passivity breakdown. Therefore, Pb particles were still present on the surface exposed to the electrolyte after the passivity breakdown and, under anodic polarization, Pb oxides were incorporated into the passive layer as suggested by Kumar et al.[18] The Cu_2O/PbO layer constituted an efficient protection against corrosion even if local corrosion phenomena were observed on the β′ phase. In contrast, at pH 12, on the pseudo-passivity plateau, the surface layer was mainly constituted of $Cu(OH)_2$ and CuO. $Cu(OH)_2$ was probably more porous and therefore less efficient in achieving a passivity of the brass than Cu_2O. The β′ phase strongly dissolved compared to pH 11 solution leading probably to the removal of lead particles. This might explain why the Pb amount of the surface layer was lower for pH 12 solution than for pH 11. The variation of Pb amount before and after the pseudo-passivity breakdown could be attributed to competition between two phenomena: the increase of the dissolution rate for the β′ phase and the increase of Pb oxidation when the anodic potential increased.

Conclusions

Results for the α,β′-brass CuZn40Pb2 in $NaNO_3$ solutions are summarized in the following points. They brought a better understanding of the corrosion processes in basic solutions of $NaNO_3$.

- At OCP, preferential Zn dissolution, promoted by the galvanic effect between the α and the β′ phases, was observed on the β′ surface. A passive layer was formed through a copper oxide layer, but lead oxide was found to participate in this passivation. The kinetics depended essentially on the pH with more dezincification for higher pHs due to the stability of Cu and Zn species.

- The anodic behavior investigated by the current density vs. potential curves was characterized by a passivity or pseudo-passivity stage followed by a breakdown. For potentials higher than the corrosion potential, the electrochemical behavior of the brass did not exclude a dezincification phenomenon, mainly of the β′ phase, but complete dissolution of this phase was predominant.

- The properties of the passive or pseudo-passive layer depended significantly on the pH of the solution and on the corresponding oxides that were formed. At pH 11, both Cu_2O and PbO were detected before and after the passivity-breakdown with only local corrosion phenomena on the β′ phase. For more basic pHs, the participation of $Cu(OH)_2$ in the oxide layer was assumed to make the oxide layer more porous and less efficient in achieving passivity of the brass. Stronger dissolution of the β′ phase leading to a removal of the lead particles should explain the absence of Pb oxides in the passive layer.

This work was performed in the framework of the CETIMAT. The CIRIMAT and the CETIM collaborate for certain aspects of their research activities; this collaboration is performed in a joint laboratory, called CETIMAT.

Acknowledgments

The authors express their sincere thanks to J. Esvan for the XPS analyses performed in the CIRIMAT laboratory.

References

1. J. Yu and R. N. Parkins, *Corros. Sci.*, **27**(2), 159 (1987).
2. J. Yu, R. N. Parkins, Y. Xu, G. Thompson, and G. C. Wood, *Corros. Sci.*, **27**(2), 141 (1987).
3. R. B. Rebak, R. M. Carranza, and J. R. Galvele, *Corros. Sci.*, **28**(11), 1089 (1988).
4. A. T. Cole, R. C. Newman, and K. Sieradzki, *Corros. Sci.*, **28**(1), 109 (1988).
5. R. M. Carranza and J. R. Galvele, *Corros. Sci.*, **28**(9), 851 (1988).
6. D. Wu, H. S. Ahluwalia, H. Cai, J. T. Evans, and R. N. Parkins, *Corros. Sci.*, **32**(7), 769 (1991).
7. F. Mackay, J. T. Evans, and R. N. Parkins, *Corros. Sci.*, **33**(5), 699 (1992).
8. E. A. Ashour and B. G. Ateya, *Corros. Sci.*, **37**(3), 371 (1995).
9. M. G. Alvarez, P. Lapitz, S. A. Fernandez, and J. R. Galvele, *Corros. Sci.*, **47**, 1643 (2005).
10. P. Lapitz, J. Ruzzante, and M. G. Alvarez, *Corros. Sci.*, **49** (10), 3812 (2007).
11. M. B. Hintz, L. J. Nettleton, and L. A. Heldt, *Metall. Trans. A*, **16A**, 971 (1985).
12. M. B. Hintz, W. K. Blanchard, P. K. Brindley, and L. A. Heldt, *Metall. Trans. A*, **17A**, 1081 (1986).
13. F. Zucchi, G. Trabanelli, M. Fonsati, and A. Giusti, *Mater. Corros.*, **49**, 864 (1998).
14. B. Assouli, A. Srhiri, and H. Idrissi, *NDT&E Int.*, **36**, 117 (2003).
15. L. Burzynska, *Corros. Sci.*, **43**, 1053 (2001).
16. A. P. Pchelnikov, A. D. Sitnikov, A. K. Marshakov, and V. V. Losev, *Electrochim. Acta*, **26**(5), 591 (1981).
17. R. H. Heidersbach and E. D. Verink, *Corrosion*, **28**, 397 (1972).
18. S. Kumar, T. S. N. Sankara Narayanan, A. Manimaran, and M. Suresh Kumar, *Mater. Chem. Phys.*, **106**, 134 (2007).
19. E. Brandl, R. Malke, T. Beck, A. Wanner, and T. Hack, *Mat. Corros.*, **60**(4) (2009).
20. E. Sarver and M. Edwards, *Corros. Sci.*, **53**, 1913 (2011).
21. C. Mapelli, A. Gruttadauria, and M. Bellogini, *Eng. Fail. Anal.*, **17**, 431 (2010).
22. C. Mapelli, D. Mombelli, S. Barella, and A. Gruttadauria, *Eng. Fail. Anal.*, **27**, 141 (2013).
23. S. A. Fernandez and M. G. Alvarez, *Corros. Sci.*, **53**, 82 (2011).
24. T. KG. Namboodhiri, R. S. Chaudhary, B. Prakash, and M. K. Agrawal, *Corros. Sci.*, **22**(11), 1037 (1982).
25. J. J. Podesta, G. P. Rothwell, and T. P. Hoar, *Corros. Sci.*, **11**, 241 (1971).
26. T. J. Kagetsu and W. F. Graydon, *J. Electrochem. Soc.*, **110**(7), 709 (1963).
27. J. Bumbulis and W. F. Graydon, *J. Electrochem. Soc.*, **109**(12), 1130 (1962).
28. H. W. Pickering and C. Wagner, *J. Electrochem. Soc.*, **114**, 7 (1967).
29. H. W. Pickering and Y. S. Kim, *Corros. Sci.*, **22**, 7 (1982).
30. H. W. Pickering, *Corros. Sci.* **23**, 10 (1983).
31. B. Assouli, PhD Thesis, (2002).
32. G. V. Korshin, J. F. Ferguson, and A. N. Lancaster, *Corros. Sci.*, **42**, 53 (2000).